

**Hydrologic Dynamics of Climate and Land-use Change: Multiple -
Resolution Modeling of the Rio Puerco River Basin, New Mexico**

Robert L Wyckoff

Advisor: Enrique Vivoni

Department of Earth and Environmental Science
New Mexico Institute of Mining and Technology
Socorro, New Mexico, 87801, USA.

For the Water Resources Research Institute at the
New Mexico State University, Las Cruces, NN

January 7, 2005

Introduction

In general, semi-arid catchments experience large variations in precipitation on timescales ranging from daily to annual intervals. These fluctuations in moisture delivered to the basin may result in substantial alterations including dynamic hydrologic response, channel erosion and arroyo channel modification, and vegetation redistribution. In order to investigate the relationships between rainfall and surface response, we have begun research using a distributed hydrologic model (Tin-based Real-time Integrated Basin Simulator) developed at The Massachusetts Institute of Technology, and employed at The New Mexico Institute of Mining and Technology for the Río Puerco Basin, New Mexico (Ivanov et al 2004, Vivoni et al, 2004a).

The Río Puerco is an ephemeral tributary of the Río Grande spanning approximately 16,160 km² with mountainous forests to the north and semi-arid desert to the south. In 2001, Mólnar and Ramírez conducted analyses of streamflow gauging stations along with a rain gauge network to determine trends in rainfall and runoff within the Río Puerco Basin. They concluded that the rainfall-runoff relationship has experienced significant changes during the latter half of the 20th century. Specifically, yearly rainfall totals have grown as a result of increased precipitation during non-summer months. Assuming constant land-surface conditions (e.g. soils, vegetation) increased precipitation should correlate to elevated streamflow. Nevertheless, the authors determine a decrease in the annual streamflow within the Río Puerco over the 50-year study period.

Mólnar and Ramírez (2001) ascribe their findings to (1) vegetation alteration influences overland flow and infiltration and (2) changes in the hydraulic characteristics modify conveyance as well as infiltration. Whether these are the primary or ancillary causes for the observed decrease in annual streamflow remains an unanswered question. Thus, the following summary discusses the initial steps undertaken to initialize a GIS based model in an effort to understand the effect of vegetation, land-use, and climate change within the Río Puerco River Basin.

In Part 1 of the paper, we discuss the initial steps taken to setup the model. The following section presents an initial tRIBS model simulation for the Upper Río Puerco. Part 3 provides analysis of large-scale atmospheric teleconnections and their relationship to streamflow at a series of locations within the Río Puerco Basin. Finally, Section 4 describes a monsoon flood event, which occurred during early September 2003.

Part 1. Model Initialization and Geographic Information Systems (GIS) Data Sets

The Tin-Based Real-time Integrated Basin Simulator (tRIBS) is a fully distributed model which prioritizes interactions between the vadose and saturated zone through the simulation of the relationship between downward moving infiltration fronts and a variable groundwater surface (Ivanov et al 2004). Thus, in order to model interconnections between the unsaturated and saturated zone, tRIBS requires accurate representation of soil, land use features, and topographic data.

Ultimately, tRIBS utilizes topographic data in the form of a triangular irregular network (TIN). The major advantage offered by the use of TINs for topographic representation is the multiple levels of resolution rendered by the irregular domain (Ivanov et al 2004). Consequently, in regions of the basin where topography is highly variable, the TIN will contain a higher density of nodes in comparison to flatter regions

where fewer nodes are required to accurately represent topography. By reducing the number of nodes in the model, the computational burden is significantly diminished.

In order to generate the model TIN, a traditional 30 m raster grid was acquired for a region slightly larger than the Rio Puerco Basin from *seamless.usgs.gov*. The raster Digital Elevation Model (DEM) was processed in Arc Hydro in order to delineate the catchment shapefile. Once the shapefile and the stream network for the entire basin were completed, the catchment was divided into its subbasins. Stream gauge and rain gauge locations were also added to the dataset. In addition, the shapefile for the continuous basin was used to clip the DEM to the basin shape (*Figure 1*).

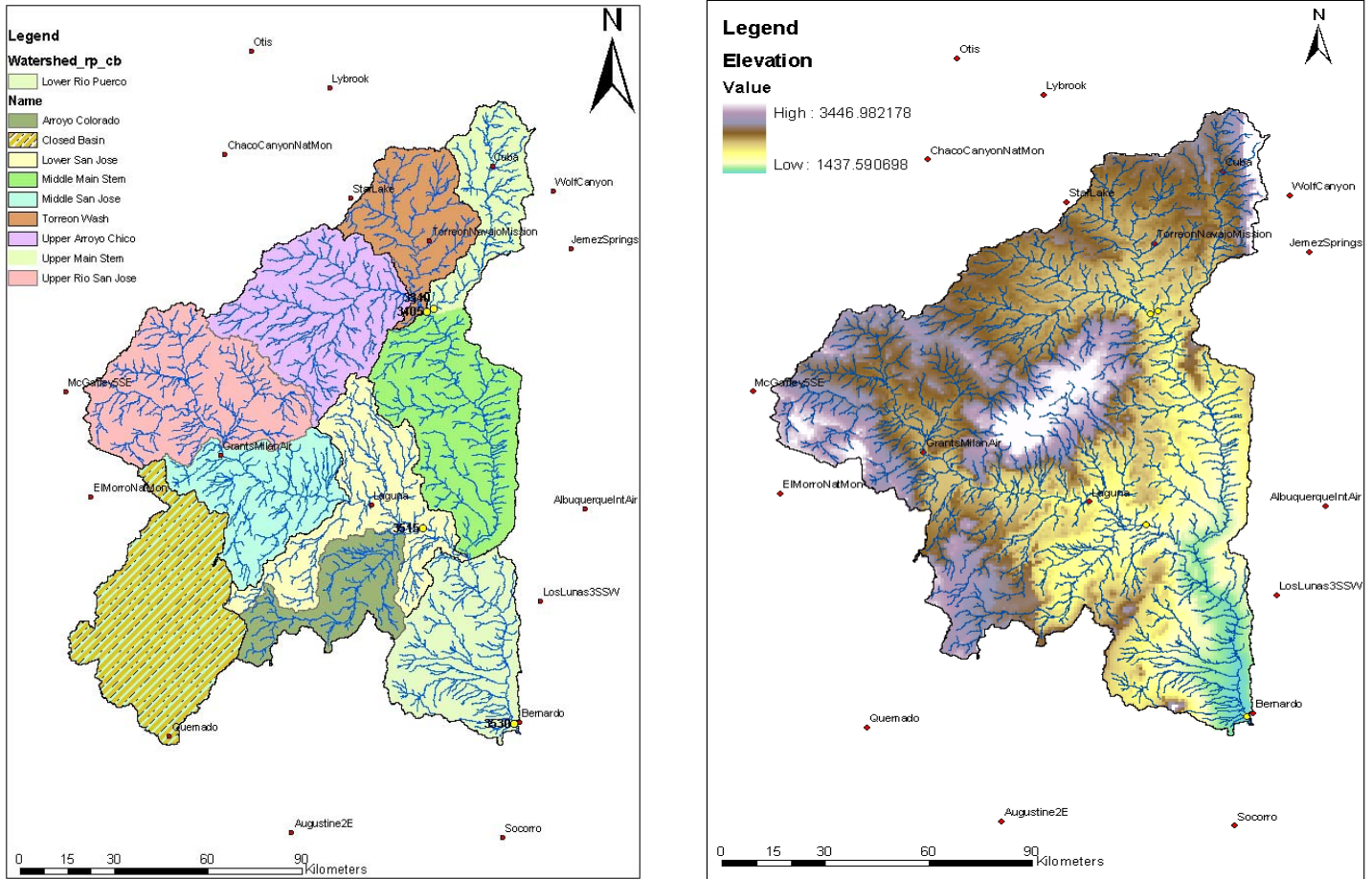


Figure 1. Rio Puerco Watershed Subbasins and Rio Puerco Clipped Digital Elevation Model (DEM). Note the closed basin shown in the left panel has been removed from the DEM on the right.

Stream Gauge	County, NM	Hydrologic Unit Code	USGS Drainage Area	Contributing Drainage Area	Gauge Elevation	Avg Yearly Rainfall (PRISM)
Upper Rio Puerco 3340	Sandoval	13020204	1088 km ²	1088 km ²	1804 m	363 mm / yr
Arroyo Chico 3405	Sandoval	13020204	3600 km ²	3600 km ²	1813 m	264 mm / yr
Rio San Jose 3515	Cibola	13020207	9479 km ²	6553 km ²	1669 m	304 mm / yr
Bernardo 3530	Socorro	13020204	18888 km ²	16109 km ²	1439 m	286 mm / yr

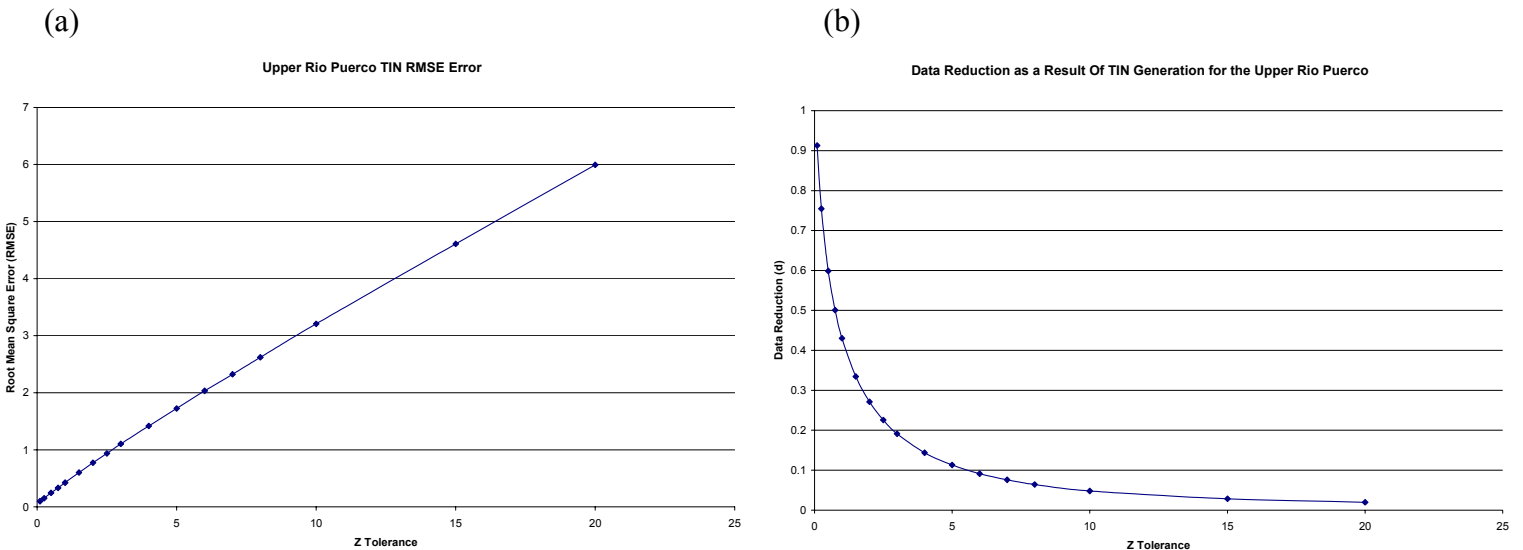
Table 1. Stream Gauge Information

The watershed consists of roughly 10 well-defined subcatchments including a closed basin located in the southwest portion of the basin. Subcatchments of greatest interest include the Arroyo Chico and Torreon Wash, the Río San Jose, the Upper Río Puerco, the Middle Main Stem, and the Lower Main Stem. Because the Upper Río Puerco exerts significant influence on the flow characteristics for the watershed as a whole, we began our modeling efforts in the northeastern portion of the catchment. Thus, the Upper Río Puerco DEM, flow direction grid, and the flow accumulation grid were extracted from the coterminous catchment since these raster grids are necessary for the TIN generation. The flow direction grid routes water from cell to cell in one of eight directions, either orthogonal to a cell edge or along a diagonal, while the flow accumulation grid assigns a value to each cell which corresponds to the number of upstream cells that flow into the particular cell of interest.

The software utilized for the TIN generation ensures that each elevation node is within a given vertical tolerance of the actual DEM value. TINs were created for tolerances ranging from 0.1 m to 20 m and the root mean square error (RMSE) for each given tolerance value was calculated. Ideally, the goal is to reduce the number of nodes required to accurately represent catchment topography, while minimizing the RMSE. In addition, we can quantify the number of nodes eliminated by comparing the nodes in the original raster to the nodes in the TIN through a data reduction factor (d).

$$d = \frac{\text{Number of Tin Nodes}}{\text{Number of Raster Nodes}} \quad (1)$$

TINs with d proximate to 1 will have a greater quantity of nodes and thus more closely approximate the original raster DEM. Therefore TINs with high d are also expected to exhibit low RMSE. The following graphic provides the data reduction vs. tolerance plot, the RMSE found for each tolerance value, and a TIN for the Upper Río Puerco with a tolerance of 20 m.



(c)

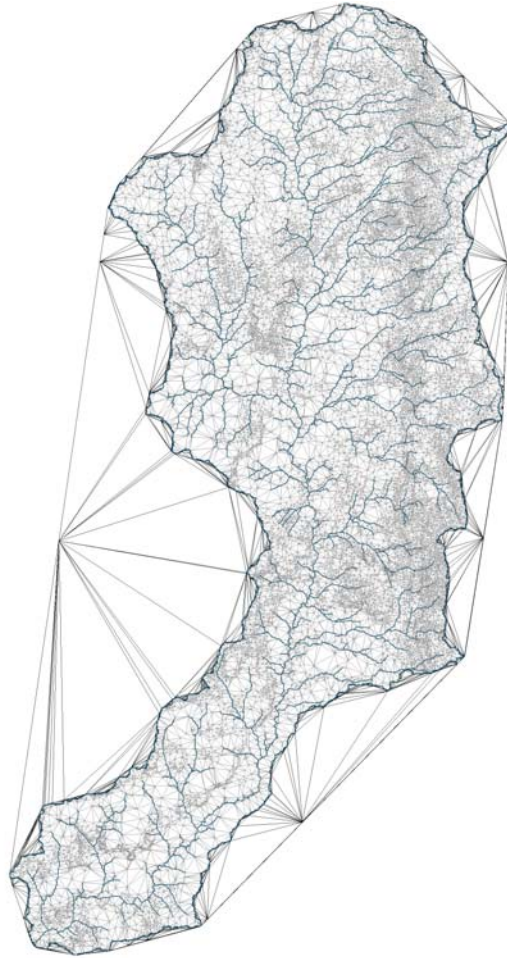


Figure 2. TINs RMSE, Data Reduction, and 20m tolerance TIN for the Upper Rio Puerco Watershed. For this TIN resolution, the data reduction factor is 2.00%.

The next step involved in model setup was to acquire soil and land use data for the Río Puerco. Again, the land use land cover data is readily available from *seamless.usgs.gov*, while STATSGO soil data is provided by the United States Dept of Agriculture Natural Resources Conservation Service. Both datasets were clipped to the Upper Río Puerco and reclassified in order to reduce both the required number of parameters and the computational burden. *Figure 3 and Table 2* below provide both data coverages and examples of parameter types along with their specified values for the model simulation. Finally, the STATSGO dataset included a depth to bedrock attribute. From this information, we populated the model with data indicating either bedrock outcrops at the surface (0m), or 5m below the surface.

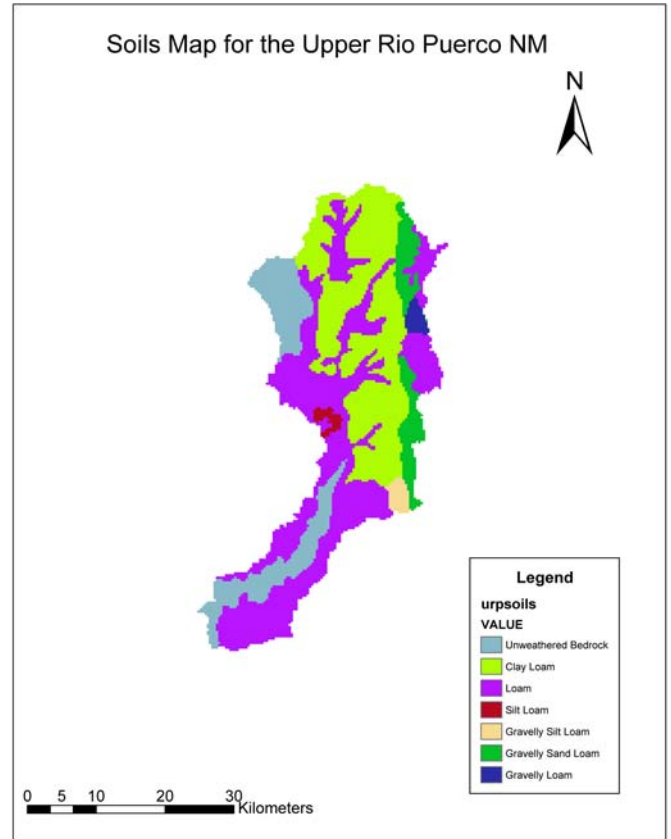
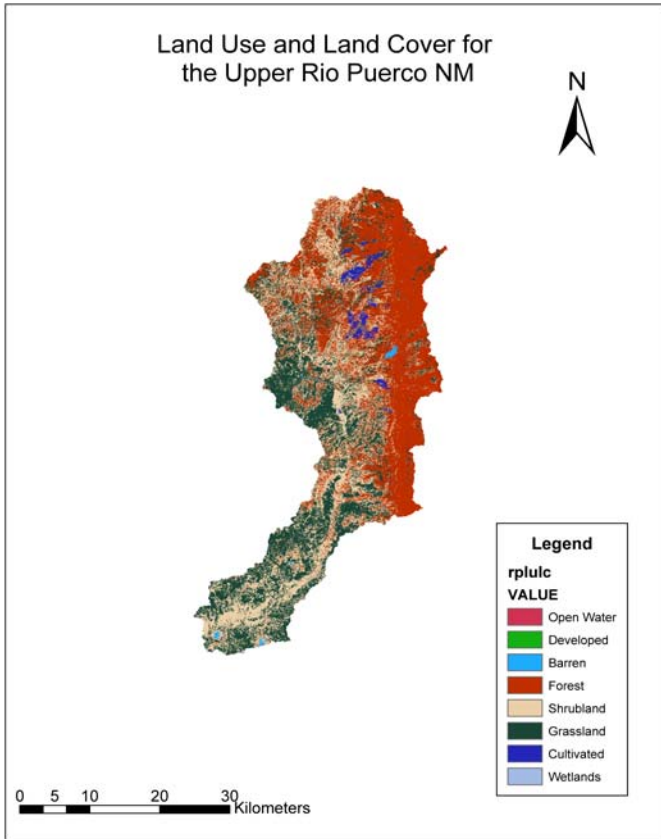


Figure 3. Land Use / Land Cover and Soil Maps for the Upper Río Puerco Watershed, NM

Parameter	Units	Soil and Land Cover Classification		
		<i>Soils</i>	<i>Sandy Loam</i>	<i>Clay Loam</i>
K_s	[mm/hr]	2.2	0.2	1.3
θ_s	[-]	0.4	0.4	0.4
θ_r	[-]	0.04	0.08	0.03
λ_o	[-]	0.38	0.24	0.25
Ψ_b	[mm]	-400	-200	-200
f	[mm ⁻¹]	0.0006	0.0004	0.0004
a_r	[-]	400	200	200
<i>Land Cover</i>		<i>Forest</i>	<i>Grassland</i>	<i>Shrubland</i>
a	[-]	0.16	0.2	0.3
h	[m]	12	0.7	1
K_t	[-]	0.8	0.9	0.9
r_s	[s/m]	60	40	50
v	[-]	0.6	0.65	0.45
c_v	[-]	Spatially-uniform, 70		
r	[-]	Spatially-uniform, 0.4		
n	[-]	Spatially-uniform, 0.3		
b	[m]	Spatially-variable, 80 m at outlet		

Table 2. Examples of simulation parameters. K_s = saturated hydraulic conductivity, θ_s = saturation moisture, θ_r = residual moisture, λ_o = pore size distribution, Ψ_b = air entry bubbling pressure, f = hydraulic conductivity decay, a_r = anisotropy ratio, a = albedo, h = height, K_t = optical coefficient, r_s = stomatal resistance, v = vegetation cover, c_v , r = non-linear routing parameters, n = Manning roughness, b = channel width. (Vivoni et al 2004b).

Part 2. Preliminary Model Results for the Upper Río Puerco

A pre-processing step in the model allowed tRIBS to construct a Voronoi Polygon Network¹ by utilizing TIN nodes as the center for each Voronoi Cell (*Figure 4*). In this case we utilized a TIN with a z tolerance of 10 m, a RMSE of 3.21 m, and a data reduction factor (*d*) of 0.048. Each parameter value at a given node is valid for the extent of the surrounding Voronoi Polygon.

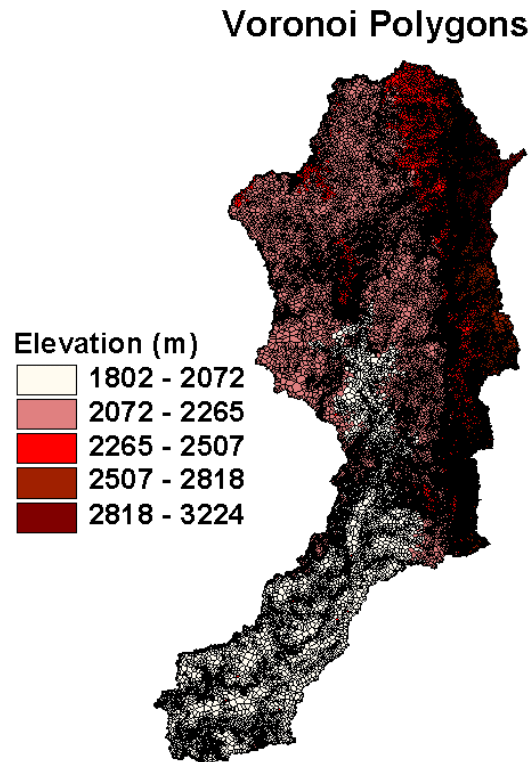


Figure 4. Voronoi Polygons for the Upper Río Puerco

Following completion of the Voronoi Polygon Network, the model was run with the soil and land use data while omitting an atmospheric forcing. The water table was placed at the land surface and allowed to drain for 3000 hrs. At the end of the simulation, baseflow conditions were achieved and the groundwater table position was used as an initial condition for subsequent model runs. Thus, the location of the water table is dependent on terrain resolution and the input parameters for the soil and land use types.

Since we lacked an extended period of NEXRAD Stage III radar data, we utilized a stochastic rainfall simulator to represent summer convective thunderstorms over the region. The simulator randomly chose duration, intensity, and time between storms based upon the parameters listed in *Table 3*.

¹ Voronoi Polygons are constructed in a manner analogous to Thiessen Polygons

Mean Rainfall Intensity (mm/hr)	10
Mean Storm Duration (hr)	2
Mean Time Interval Between Storms (hr)	24

Table 3. Stochastic Rainfall Simulator Parameters

Rainfall was uniform throughout the basin and resulted in an outlet hydrograph with very quick ascending limbs as well as rapidly falling descending limbs (*Figure 5*). In addition to generating outlet hydrographs, tRIBS also possess the capability of recording discharge estimates at internal nodes. *Figure 5* also shows the location of two internal stream nodes and their corresponding stream hydrographs.

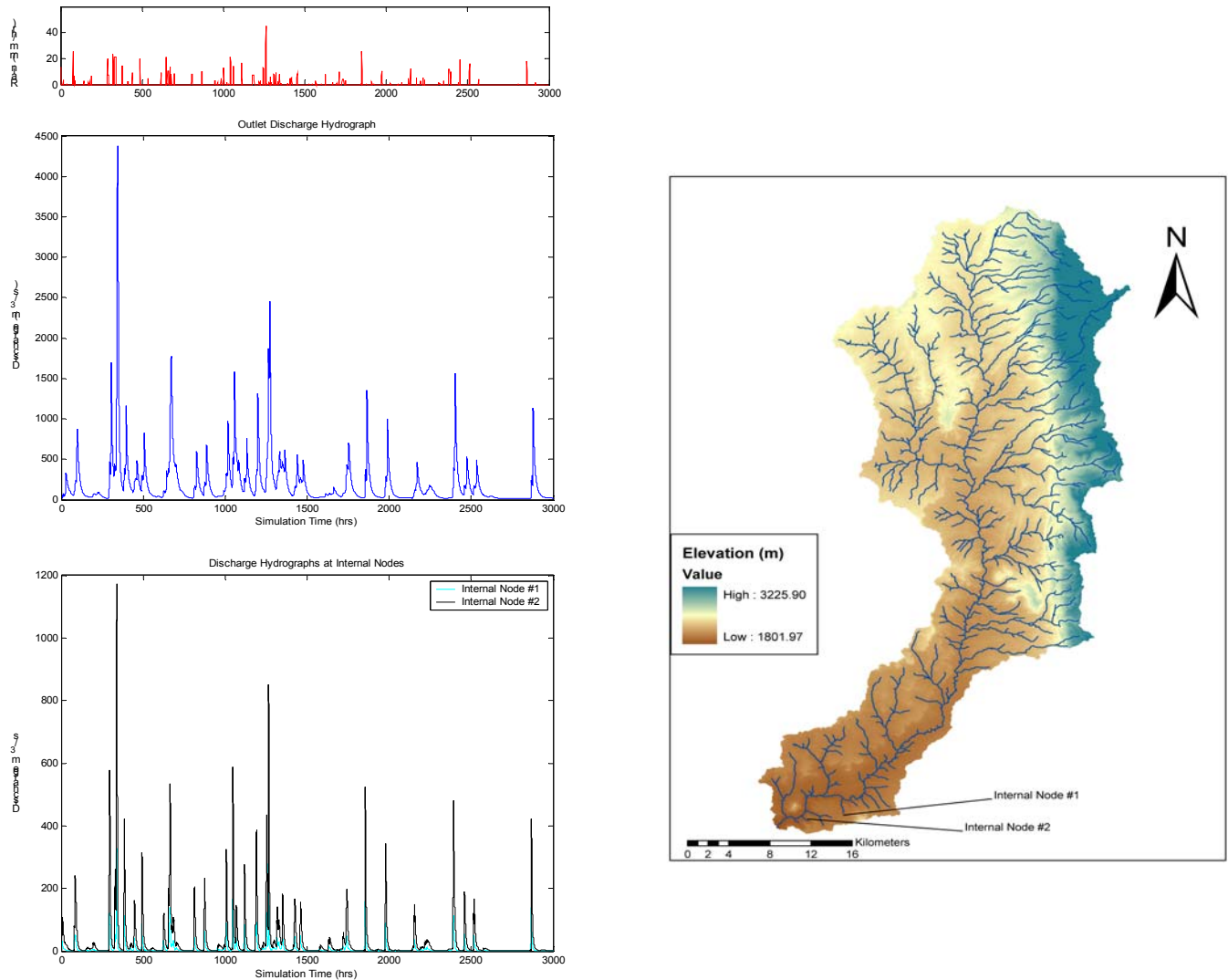


Figure 5. Stochastic simulated rainfall and outlet discharge as well as internal node discharge for summer convective thunderstorms. Note the location of internal nodes are given in the right panel.

Finally, tRIBS is able to output data related to the internal catchment dynamics at both varying temporal and spatial scales. For example, *Figure 6* demonstrates time-averaged root zone soil moisture over the entire simulation period as well as the shallow

ground water table following the 3000 hr simulation. Higher regions of soil moisture are located in regions of bedrock outcrops with lower soil moisture located predominantly along the catchment's eastern boundary. These regions of low soil moisture correspond to a greater depth to water whereas regions approaching saturation exhibit minimal depth to the water table. It is readily evident that soil properties are dictating soil moisture distribution within the watershed.

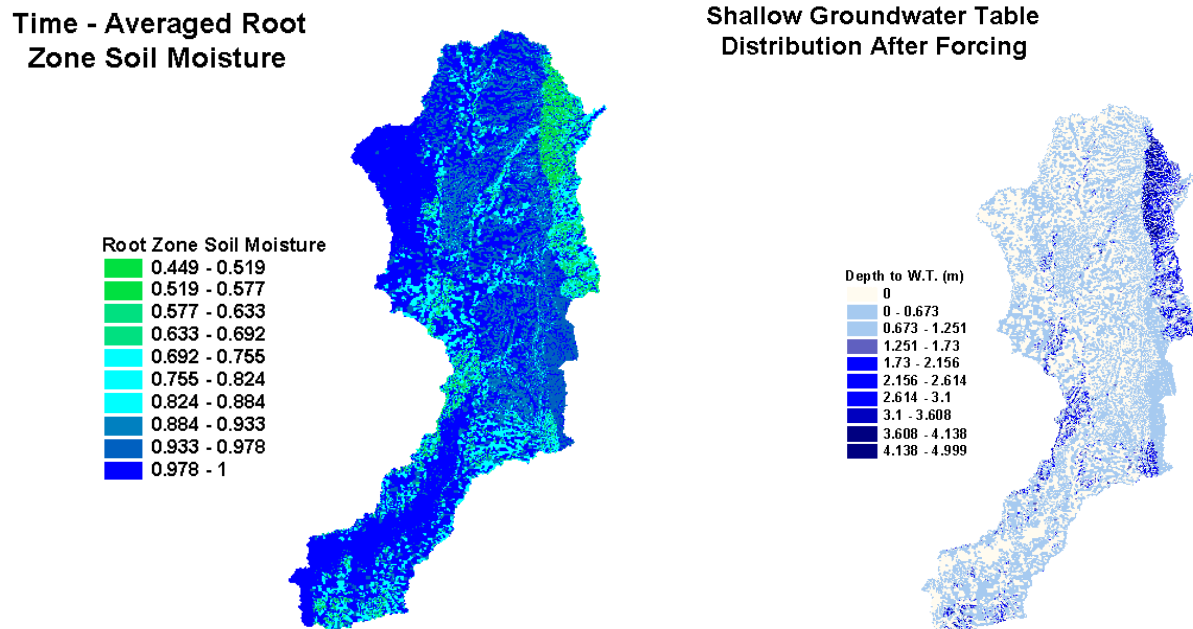


Figure 6. Spatial representation of root zone moisture (top 1 m) during simulation period as well as spatial map of depth to groundwater table (m) at $t = 3000$ hrs

Future Work

In order to achieve greater physical representation of actual catchment processes, we need to gather NEXRAD Stage III radar data to allow an extended period of atmospheric forcing. Ideally, a period of prolonged dry conditions followed by a rainfall or series of rainfall events would allow the model to accurately represent basin dynamics since baseflow and internal catchment properties may be captured prior to the storm event simulations. In addition to rainfall data, soil and land use parameters need to be verified. Specifically, the model currently becomes saturated in regions of bedrock outcrops. The model fails to route water quickly away from these regions suggesting the saturated hydraulic conductivity parameter for bedrock should be set to zero. Finally, the model is capable of producing extensive spatial maps including evaporation from soil, transpiration, heat fluxes, and runoff types (infiltration excess, saturation excess, perched return flow, and groundwater exfiltration). These processes are of interest but the data need to be extracted from the model. Furthermore, these results are of little utility until the model can be properly executed and calibrated. Thus we also need extended stream

discharge data from the Upper Río Puerco at Guadalupe streamgauge (3340). Streamflow data will provide the standard to which we can compare our simulated discharge results and thereby calibrate the model.

Part 3. Hydroclimatology of the Río Puerco

A pervasive issue in the desert southwest, and especially in New Mexico, is the issue of water availability and the subsequent economic and social impact of its limited availability. Many communities in the West currently rely on reservoirs replenished primarily from snowmelt during a seasonal period in which water demand is typically low. Therefore water managers must apportion resources arriving in periods of high flow to the summer season in order meet peak water demands. The successful operation of these reservoirs is ultimately dependent on informed decisions accounting for future variations in climate and the hydrologic cycle.

Thus, the focus of this portion of the study centers on the predictive capabilities of two climate indices for future streamflows in the Río Puerco Watershed, New Mexico. Specifically we utilize time series analysis using historical stream flow records at four stations within the watershed along with an El Niño / Southern Oscillation and Pacific Decadal Oscillation Indices to identify relationships between climate forcing and streamflow in a complex basin.

El Niño / Southern Oscillation and Pacific Decadal Oscillation

The Southern Oscillation is a large-scale ocean-atmospheric interaction that occurs over the equatorial Pacific capable of modifying global climate. Traditionally, high pressure is centered over the South Pacific near Tahiti with lower pressure entrenched over Indonesia and Australia. The strength of the pressure gradient is associated with the intensity of the trade winds which blow from east to west along the equator. These atmospheric patterns tend to push warm ocean water away from the western coast of South America and toward Eastern Asia and Australia. As the pressure gradient in the Western Pacific decreases, so do the trade winds and warm water is allowed to accumulate off the Peruvian coast. The warm water offshore of South America promotes atmospheric conduction leading to thunderstorm formation and frequent flooding in Peru while the Western Pacific is dominated by cooler ocean water and abnormally dry climatic conditions. These altered trends in pressure and temperature gradients also deflect the jet stream over North America to the south resulting in increased rainfall for many traditionally arid areas and drought in normally productive agricultural regions (*Dingman 2002*).

Two different indices are available for characterizing ENSO – sea surface temperature (SST) anomalies and the Southern Oscillation Index (SOI). SST is calculated as the divergence from the long-term mean in oceanic surface temperature averaged over a well-prescribed region of the eastern and central equatorial Pacific Ocean (*Amarasekera et al 1997*). Alternatively, SOI is determined as the difference in standardized sea level pressure between Tahiti, French Polynesia and Darwin, Australia. A large positive SOI index reflects a La Niña year while a large negative value is indicative of an El Niño event (Figure 7).

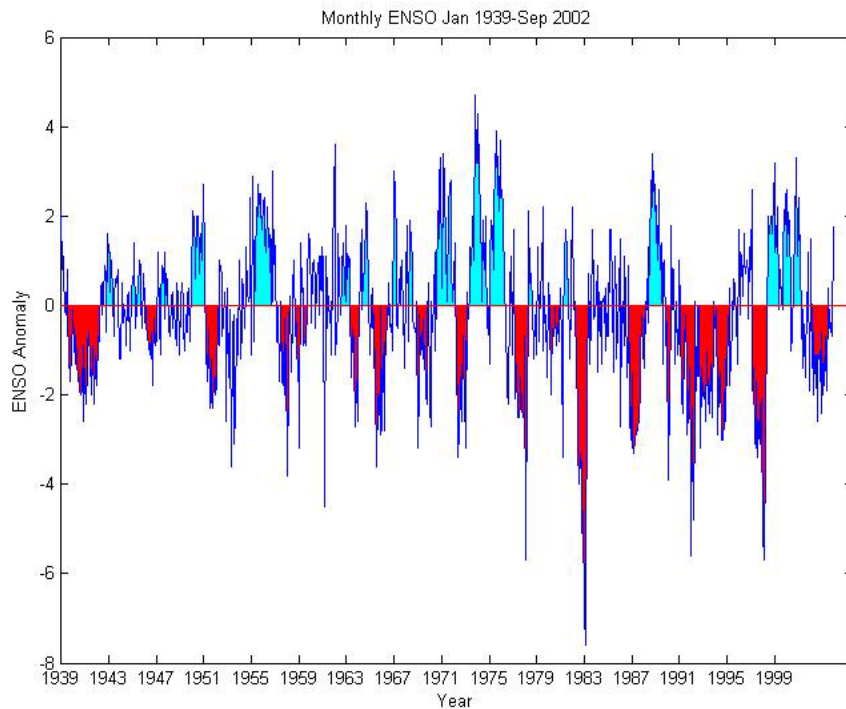


Figure 7. Fluctuations in ENSO as Captured by the SOI Index; red = El Niño while light blue = La Niña

Numerous studies have documented the correlation between ENSO and precipitation and river discharge respectively in various locals around the world. *Amarasekera et al (1997)* employed SST as an index for ENSO and determined a positive correlation between discharge in southeastern South America's Paraña River and El Niño episodes. In contrast, two major tributaries of the Nile River, the Atbara and Blue Nile, were found to exhibit a significant negative correlation with the ENSO phenomenon. *Wang and Eltahir (1998)* expanded on this work using rainfall, river flow, and ENSO events to conduct medium and long-range predictions for the Nile River flood. When forecasting for periods larger than the hydrological response timescale, ENSO was the principal governing parameter required to achieve accurate forecasts. As the prediction time approached the hydrologic response interval, rainfall and river flow data became more important in achieving accurate flood forecasts.

The Pacific Decadal Oscillation (PDO), shown in *Figure 8*, is another climate forcing phenomenon that has similar spatial climatic influences as the El Niño/Southern Oscillation. Unlike ENSO which may persist for 6 to 18 months, the PDO period can perpetuate for 20 – 30 years. (*Mantua 2000*). The warm phase of the PDO is characterized by abnormally warm SSTs along the west coast of North America, relatively cooler SSTs in the central Pacific, and a drop below average pressure in the North Pacific. Indices capturing the PDO based on either sea level pressure (SLP) or SST are positive for warm PDO episodes. Over the past century there is only evidence for two full PDO cycles – cool phases occurred from 1890 – 1924 and from 1947-1976 while warm episodes were entrenched from 1925-1946 and from 1977 through at least the mid 1990s (*Mantua, 2000*).

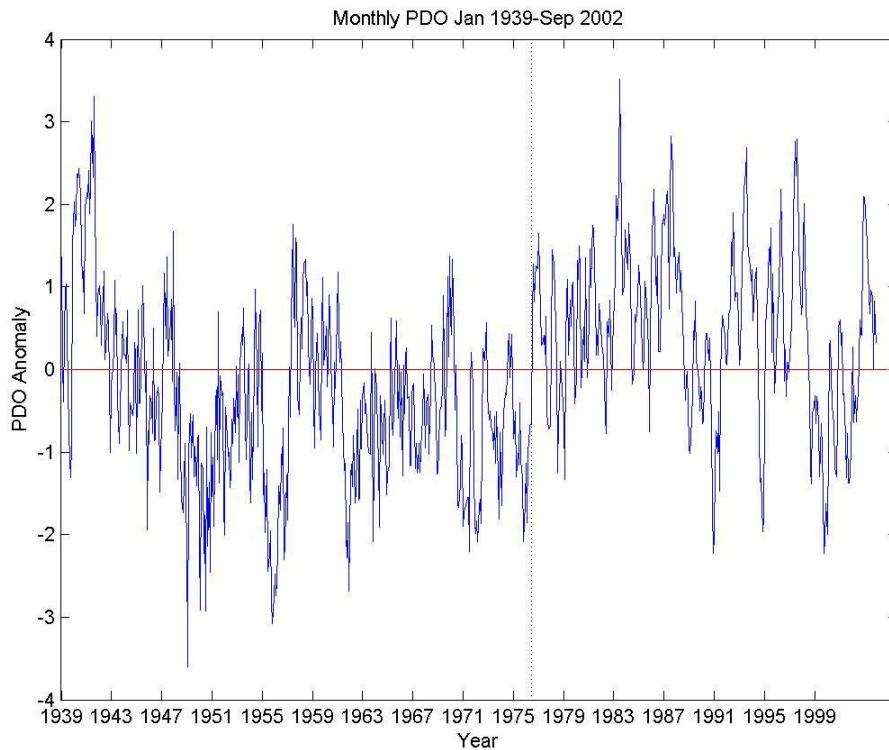


Figure 8. Fluctuations in the PDO Anomaly. Values above the red line correspond to warm phase PDO while values below the line are cold phase PDO. Dotted black line indicates PDO climatic regime shift (1977)

Large Scale Atmospheric Circulation and Climatic Variability in the Southwest

In recent years, studies have investigated the possibility that the Southern Oscillation is correlated to variability in the Southwest's regional climate including temporal fire patterns, streamflow, precipitation, and drought. For example, *Lough and Frits (1985)* demonstrated that because low SO Index years were closely related to wet winter conditions in the Southwest, tree ring chronologies could be utilized to reconstruct the climatic shifts within the historical record when meteorological observations are unavailable. *Swetnam and Betancourt (1990)* applied this work by quantifying tree ring width and tree ring fire scars in order to recreate a fire history for forests in New Mexico and Arizona. They found the area of burned woodland was greatest during time periods preceded by high values of the SOI. Time periods characterized by wide tree rings were marked by less evidence of scarring from fire. Since Douglas-fir and Ponderosa Pine exhibit the greatest cambial growth when receiving rainfall in the autumn and spring prior to the growing season, wide tree rings may provide an indication of El Niño periods.

Redmond and Koch (1991) reinforced the notion that precipitation in the southwest was significantly interconnected to fluctuations in the ENSO. They determined the highest correlation coefficients between SOI and precipitation occurred when an averaged SOI period preceded rainfall by less than four months. Their negative

correlation coefficients explained as much as 33% of the variance in winter precipitation within certain Southwest climate divisions. The negative sign on the correlation coefficient suggests that larger than average winter precipitation is more strongly related to El Niño events in the equatorial tropics. These results support the conclusion that ENSO strongly affects the southwestern hydrologic cycle; however, long term forecasting should also include measurements of the Pacific Decadal Oscillation.

For example, *Gutzler et al (2002)* employed measurements of predictive skill to quantify the accuracy of forecasted precipitation based upon various climate forcing indices. Their results suggest predictions possess greater accuracy for cold ENSO indices followed by dry winters in comparison to warm ENSO indices succeeded by wet winters prior to the 1977 PDO climate regime shift². After the mid 1970s climatic adjustment, predictive skill experienced a reversal – that is El Niño years proved more accurate indicators of seasonal climate than La Niña episodes. However, when compared with an ENSO index, the PDO accounted for little predictability of anomalous Southwest winter precipitation. So while it is important to include the PDO index in the analysis to discriminate which ENSO event will allow accurate seasonal precipitation forecasts, PDO does not singularly enhance climate predictions within the Southwest.

While precipitation is strongly correlated to ENSO, the same results have not been demonstrated for periods of drought. *Piechota and Dracup (1996)* determined that drought corresponded to signals in ENSO only in the Pacific Northwest and Southeastern United States. In the Northwest, three of the largest droughts from 1900 to 1993 occurred immediately following El Niño events. While no significant correlations existed between drought and the ENSO in New Mexico, *Piechota and Dracup (1996)* did observe increased rainfall in southeastern New Mexico and Texas associated with the occurrence of El Niño.

In North America, *Kahya and Dracup (1994)* analyzed the influences of Type 1 El Niño events (T1ENSO) on streamflow in the Southwest United States. T1ENSOs occur during the months of June through August and are characterized by warmer than normal surface water east of the International Date Line, typical conditions in the west Pacific, with the warmest ocean temperatures spanning the eastern Pacific from 150° – 160° W longitude. *Kahya and Dracup (1994)* found elevated stream discharge during the months of December-July was significantly related to the occurrence of Type 1 El Niños. *Redmond and Koch (1991)* also found stream flow in the Southwest demonstrated a negative correlation to SOI from the prior summer and fall season.

² *Minobe (1997)* defines a climate regime shift as “a transition from one climatic state to another within a period substantially shorter than the lengths of the individual epochs of each climate state”

Data Collection and Methodology

Daily discharge data for each of the four stream gauges was downloaded from the National Water Information System website (NWIS). At Bernardo, NM, average daily discharge is available from Jan 1, 1954 through September 2002. Data from all gauges was downloaded as a tab delimited text file and superfluous data was removed in Excel. The Río San Jose at Correo, NM has discharge records from April 1, 1943 through September 30, 1994 while the Río Puerco above Arroyo Chico has historical data from October 1, 1951 through September 30, 2002. Finally, the Arroyo Chico stream gauge provides records from October 1, 1943 through September 30, 1986 (See Figure 1 for location of gauges within the Rio Puerco watershed).

Southern Oscillation Index values from January 1882 through January 2004 are available from the Climate Prediction Center. The SOI is calculated via the following steps

$$\text{Standardized Tahiti} = \frac{(\text{Actual Tahiti SLP} - \text{Mean Tahiti SLP})}{\text{Standard Deviation Tahiti Anomaly}}$$

$$\text{Standardized Darwin} = \frac{(\text{Actual Darwin SLP} - \text{Mean Darwin SLP})}{\text{Standard Deviation Darwin Anomaly}}$$

$$\text{Monthly Standard Deviation} = \text{SQRT}((\text{Standardized Tahiti} - \text{Standardized Tahiti})^2 / N)$$

where N is the total number of summed months. Then the Southern Oscillation Index

$$\text{SOI} = (\text{Standard Tahiti} - \text{Standardized Darwin}) / \text{MSD}$$

where MSD is the monthly standard deviation.

The PDO developed by Nathan Mantua at the University of Washington is calculated using the UKMO Historical data set for 1900–1981, the Reynolds's Optimally Interpolated SST (V1) for January 1982–Dec 2001, and OI SST Version 2 (V2) beginning January 2002 to current.

In order to analyze the data, daily monthly flows for December, January and February were summed using a Matlab code to provide total winter flow for each year of the stream gauge record. The identical procedure was performed over the months of June, July, and August to generate total flow over the monsoon/summer season. The SOI index was divided into the following seasonal bins and averaged – December January February (DJF); March April May (MAM); June July August (JJA) and September October November (SON). A Matlab code calculated the correlation coefficient (R) for either monsoon or winter discharge and the SOI from the season of interest. For example, if we were interested in the correlation between winter streamflow and the previous summer's ENSO characteristic over a forty year period, we would have 40 averaged SOI values for JJA and 40 DJF flow sums from which R is calculated. Rather than calculate R merely over the entire continuous history for each respective gauge, we also divided the SOI and Daily Discharge record into segments prior to and following the

1977 PDO climatic regime shift. Since the ENSO and PDO are correlated phenomena we would expect different R values corresponding to the different phases of the PDO. The correlation coefficient squared can be interpreted as the percentage of variance in flow explained by ENSO events.

Results and Interpretation

Rio Puerco at Bernardo

Figure 9 shows the correlation coefficients for SOI bins up to 30 months previous to the flow period of interest over both winter and summer flow periods. Maximum seasonal SOI correlations with winter flow over the entire record occur in the DJF months concomitant to flow period as well as the SON months immediately prior to winter streamflow. However, the SOI explains only 5% of the total variance in streamflow. The consistent negative sign of correlation coefficients over the continuous flow period suggests a low SOI value (indicative of an El Niño event) is weakly associated with increased flow.

Dividing the winter flow and SOI record based upon the PDO climatic regime shift did not substantially increase the predictive capability of climate indices for streamflow over any of the preceding seasonal periods for years prior to 1977. Following 1977, ENSO conditions during the DJF season 12 months preceding the winter flow period of interest reached a maximum at $R = -0.300$. This weak correlation between ENSO and winter discharge does not allow future predictions of streamflow with any greater confidence than that of the annual flow mean taken over the historical record.

Strong correlations between SOI and Monsoon flow at Bernardo are non-existent when looking at the entire record or the duration prior to 1977. However for years following 1977, the DJF average SOI 18 months prior to the Monsoon explains 14% of the variance in streamflow during the summer months. This correlation is still too weak to enhance predictive aptitude with confidence.

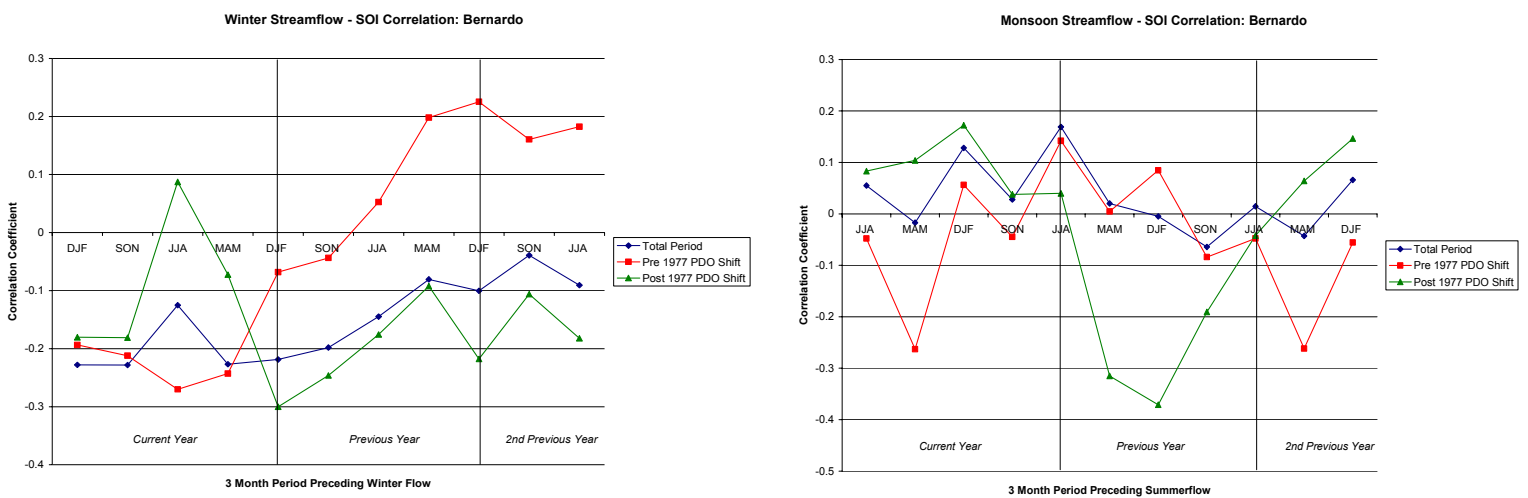


Figure 9. Correlation Coefficients for Winter and Summer Stream Discharge and ENSO indices at Bernardo, NM.

Rio San Jose at Correo

In *Figure 10*, winter discharge in the Rio San Jose at Correo from 1943 – 1994 is weakly correlated with SOI Index. Dividing the dataset into pre and post PDO climatic regimes increases the value of the correlation coefficients for periods prior to and following 1977. From 1934 – 1977, correlations between streamflow and SOI were strongest twelve to twenty one months prior to the period of discharge. SOI for SON 15 months prior to winter streamflow explained a maximum of 12% of the observed variance over the subset time period. After 1977, the MAM period six months prior to winter discharged had a maximum R value of 0.3398 ($R^2 = 12\%$). Both before and after the PDO shift, increased streamflow was slightly correlated with periods of La Niña.

SOI values over all years at the Rio San Jose were weakly correlated with monsoon flow in June July and August. This same trend was repeated when analysis was performed on the years preceding 1977. However after the phase shift in PDO a relatively stronger correlation ($R^2 = 17\%$) emerged in the DJF SOI index 3 months prior to the monsoon period of interest. When compared to other studies however, this correlation coefficient appears insignificant.

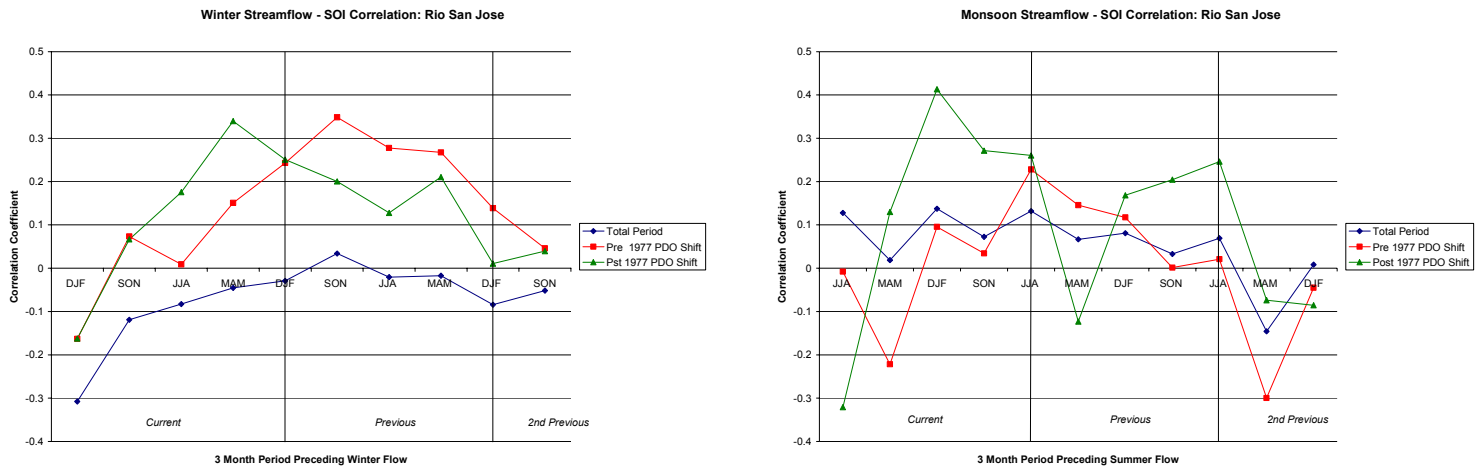


Figure 10. Correlation Coefficients for Winter and Summer Stream Discharge and ENSO indices for the Rio San Jose at Correo, NM.

Arroyo Chico

Figure 11 presents winter stream flow correlation with average seasonal SOI. From 1943 – 1986 approximately 10% of the variance in streamflow is explained by SOI during DJF, JJA, and MAM periods between 12 and 24 months prior to the winter discharge. The maximum correlation coefficient prior to 1977 indicates 12% of the variance in stream flow may be attributed to MAM SOI 21 months prior to winter flow. During these twenty-seven years, correlation coefficients are predominantly positive suggesting increased streamflow is related to La Niña events. Correlation Coefficients post 1977 and immediately preceding winter flow are either weakly positive or almost zero. However, when we look at periods greater than 1 yr in advance of streamflow we see the development of a relatively strong persistent negative correlation between SOI

and winter discharge. The maximum explanation of variance (27%) occurs for MAM SOI 18 months prior to the summation of flow period. An additional high correlation ($R^2 = .23$) is observed in JJA period 30 months prior to the winter flow for time periods following the 1977 regime shift.

Figure 11 also plots the correlation coefficients between SOI and summer flow over the entire historical period as well as the two temporal subsets based upon the PDO. No significant correlations exist between ENSO and monsoon flow within the Torreon Wash or Arroyo Chico subwatersheds for most of the SOI seasons. However, the post 1977 MAM SOI bin immediately preceding the monsoon season explains 27% of the variance seen in the monsoonal stream flow at Arroyo Chico. Note only 9 data points fall after the 1977 PDO shift for the Arroyo Chico stream gauge. Thus these regression values are calculated based upon a very limited dataset and it is probably best to disregard this strong correlation during MAM.

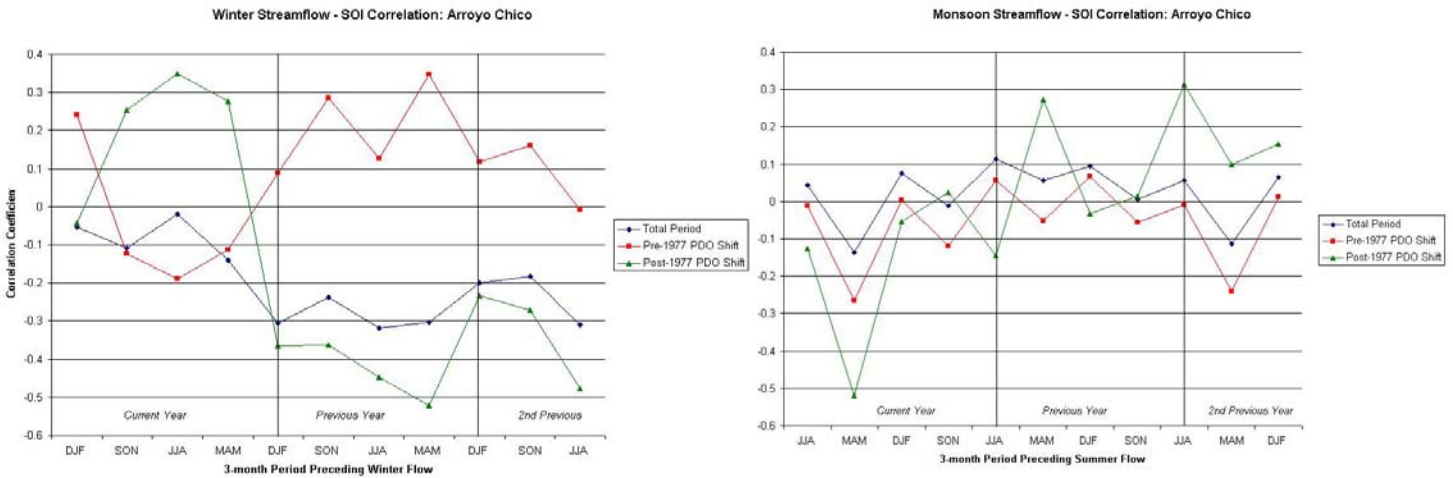


Figure 11. Correlation Coefficients for Winter and Summer Stream Discharge and ENSO indices for the Arroyo Chico.

Upper Rio Puerco

The Upper Río Puerco shows little correlation between SOI and winter flow when the entire historical record is considered (Figure 12). Dividing the streamflow record according to the PDO shift of 1977 results in slightly stronger correlations but these remain relatively insignificant. The maximum explanation of variability in streamflow is only 13% and occurs in the pre-regime shift plot during the MAM period 21 months previous to the winter flow event.

Unlike the Arroyo Chico discharge, monsoon flow in the Upper Río Puerco is strongly correlated to SOI in the years following 1977 relative to other observed correlations. Specifically the MAM season 12 years prior to the monsoon period explains 22% of the variability in summer streamflow (Figure 12).

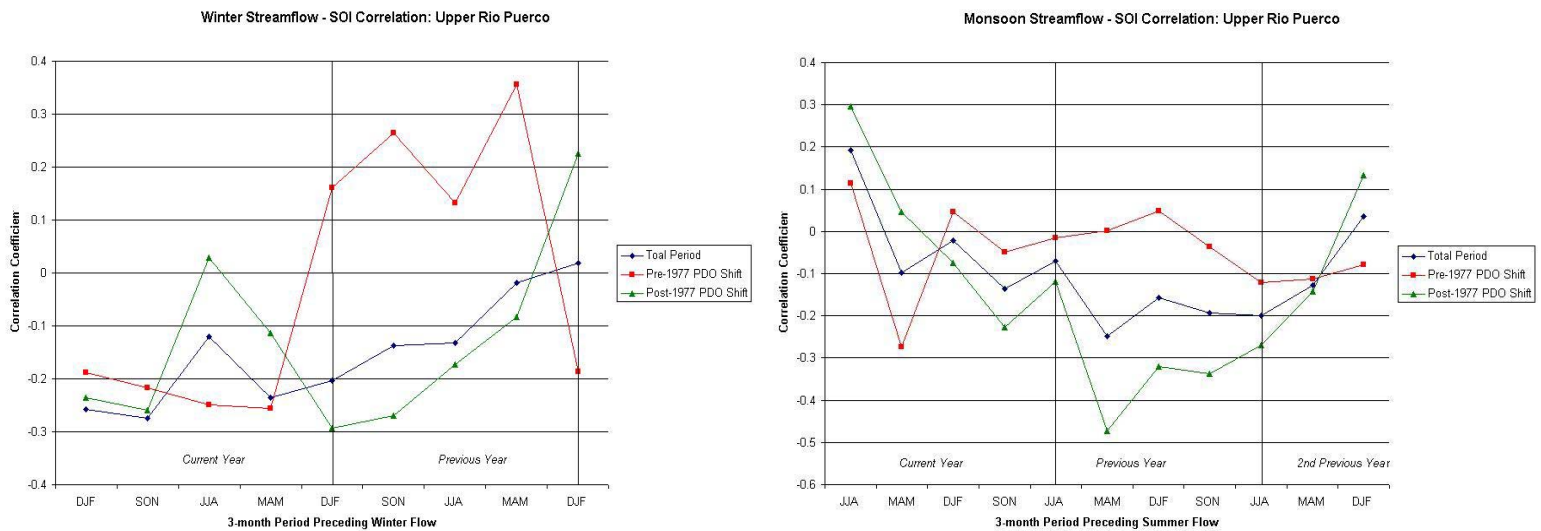


Figure 12. Correlation Coefficients for Winter and Summer Stream Discharge and ENSO indices for the Upper Rio Puerco.

Conclusions

Based upon simple linear regression techniques we were not able to verify streamflow at different gauges for different times of the year were consistently related to variations in ENSO even when we accounted for shifts in the PDO Index. At Bernardo and Río San Jose, correlations were weak and therefore accounting for ENSO in predicting future stream flows would not contribute to greater forecasting accuracy.

Within the literature, strongest correlations between winter stream flow and ENSO usually occur utilizing SOI data from the year leading up to the flow period of interest. Our study at Arroyo Chico and the Upper Río Puerco indicates it may be necessary to look at ENSO further back in the historical record in order to find stronger correlations which could be used to enhance prediction accuracy of future streamflow.

Although our correlations often did not provide convincing explanation of variance in streamflow, we uncovered a few interesting findings. For example, correlations increase between monsoon stream flow and ENSO in both the Arroyo Chico and the Upper Rio Puerco following the 1977 regime shift. However, the correlation between monsoon and ENSO in the Arroyo Chico is isolated to a three month stretch of MAM immediately prior to the discharge record and based upon a limited data set. If we ignore this SOI period, little correlation is evident between monsoon streamflow and ENSO within this sub basin. This is in contrast to the neighboring Upper Río Puerco watershed in which elevated discharge is consistently related to El Niño from 15 to 24 months prior to the summer flow period. Again for dates post the 1977 PDO shift, the relationship reverses in the winter months when flow in the Arroyo Chico is strongly correlated to ENSO from one to two years earlier and little to no relationship between SOI and winter discharge is observed in the Upper Río Puerco. The finding that winter flow is correlated with El Niño in the Arroyo Chico is consistent with previously published research however the correlation between monsoons and SOI is unsubstantiated by preceding work.

Another interesting result is that the only strong correlations between ENSO and stream discharge were observed following the 1977 shift in PDO. Thus warm phases of PDO may provide greater confidence in the future prediction of streamflow within the northern reaches of the Río Puerco Watershed. More importantly however, if we had merely looked at the stream flow record over the entire historical record, the relatively high correlation coefficients observed in the Arroyo Chico and Upper Río Puerco following 1977 would have passed unnoticed. An additional outcome of dividing the record based upon PDO is that high winter flows in the Arroyo Chico were weakly correlated with La Niña prior to 1977 but following the regime shift large DJF discharge was correlated with El Niño. Thus the correlation relationship between ENSO phase and streamflow may vary in sign depending on PDO phase shifts (See *Figure 8* Arroyo Chico Winter Flow Previous Year). The finding that ENSO should be analyzed along with a PDO component supports the research of *Gutzler et al (2002)*.

It appears from this study, high mountainous catchments in North Central New Mexico are more responsive to changes in ENSO than stream gauges draining large surface areas. This finding is supported by *Redmond and Koch (1991)* who discovered the Gila River shows statistically significant negative correlation with SOI from the previous summer and fall seasons. This correlation is not seen at lower elevations for the Río Puerco since the stream is losing water - the water table does normally intersect the streambed and subsequently flow is lost to infiltration. This could result in correlation between ENSO and headwater catchments that is not observed at the drainage outlet. For this watershed, since the upper tributaries respond in different seasons to shifts in ENSO, El Niño years may exhibit more continuous flow in the lower reaches than in modal or La Niña episodes. This hypothesis will require further investigation.

Future Work

In order to further analyze the relationship between ENSO, PDO, and streamflow in the Rio Puerco Basin, we would like to employ a more sophisticated statistical technique. For example, Wang and Eltahir (1999) use spectral analysis to enhance long range forecasting of Nile River Floods. An alternative option would be to use a harmonic analysis technique. Kahya and Dracup (1993), Piechota and Dracup (1996), and Chiew and McMahon (2002) used harmonic analysis to determine associations between ENSO and drought, US patterns in streamflow, and global patterns in streamflow respectively.

Part 4. Monsoonal Flood Events in the Río Puerco Basin

The North American Monsoon is a late summer atmospheric circulation pattern which spawns convective thunderstorms and thereby substantially influences precipitation in both northwestern Mexico and the southwest United States. In New Mexico, rainfall events during the months of July, August, and September account for roughly 40 – 55% of the total annual precipitation. (*Douglas et al.*, 1993). These thunderstorm events can result in flood events for both perennial and ephemeral rivers and streams.

From September 4 – 11, 2003 a series of storm events swept across the northern regions of the Río Puerco Basin resulting in flash flooding extending through the catchment and into the Río Grande. USGS stream gauges both interior to the basin and along the Río Grande allow quantification of the flood wave through the Río Puerco Basin into a major river system. The goal is to interpret the conversion of a monsoon storm system into a large flood event within a semiarid ephemeral tributary and the subsequent implications for a major river system.

Data Sets

Currently within the Río Puerco Basin, streamflow measurements are recorded at two gauging locations: Río Puerco at Guadalupe, NM (3340) and Río Puerco at Bernardo, NM (3530). The United States Geological Survey (USGS) provided river stage and discharge estimates at 15 min resolution for both locations. Manual measurements performed vial flume and cableway by the USGS verified the accuracy of gauge discharge estimates. In order to investigate downstream effects of the Río Puerco flood, USGS river stage and discharge data was also gathered for the Río Grande both upstream and downstream of the Río Puerco confluence: Río Grande at Albuquerque, NM (3300); Río Grande at Bernardo, NM (3320); Río Grande at San Acacia, NM (3549); and Río Grande at San Marcial, NM (3584).

Both ground based and remote sensing instrumentation allowed precipitation estimation within the basin. Eighteen rain gauges are located within the region of which only four (Cuba, Torreón, Grants, and Laguna) lie inside the Río Puerco Watershed. Raingauges in the region record data at daily, hourly, and 15 min time scales depending on location. We were also able to utilize Stage III radar product at 4km x 4km resolution for the Río Grande Region. Radar estimates were supplemented with satellite cloud imagery from GOES (Geostationary Operational Environmental Satellite), regional surface weather observations and upper air charts from Unisys Weather (<http://weather.unisys.com>) to form a conceptualization of atmospheric conditions leading to the monsoon flood event (*Vivoni et al 2004c*).

Results

The flood frequency curve at Bernardo (*Figure 13*) demonstrates that when placed in context of the historical record, the September 2003 flood was not especially large. However, in recent times the annual maximum flood has steadily decreased over time (*Figure 13*). Thus, either atmospheric forcing or basin characteristics (channel

geometry, vegetation, landuse, etc) have led to a changing hydrologic response from the basin.

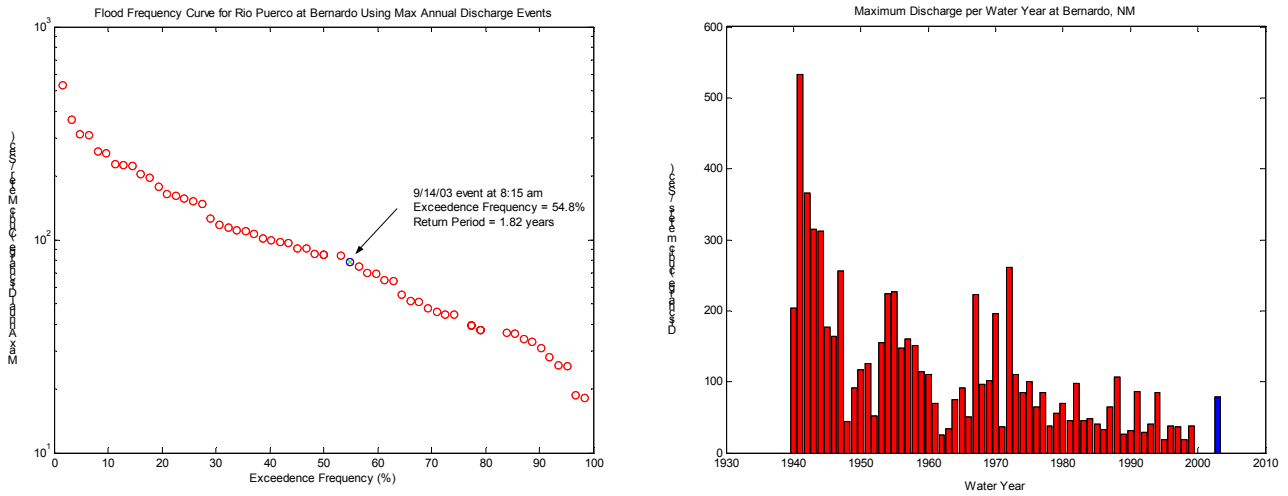


Figure 13. Flood Frequency Curve and Annual Peak Discharge: Rio Puerco at Bernardo, NM. In the annual peak discharge plot the Sep 2004 event is shown in blue.

Raingauge and radar data from the region demonstrate the primary areas of heavy rainfall resulting in the Río Puerco flood occurred in the northern extent of the watershed. The following figure provides total rainfall depths for both raingauge measurements and hourly radar estimates from September 6 – 18 2004.

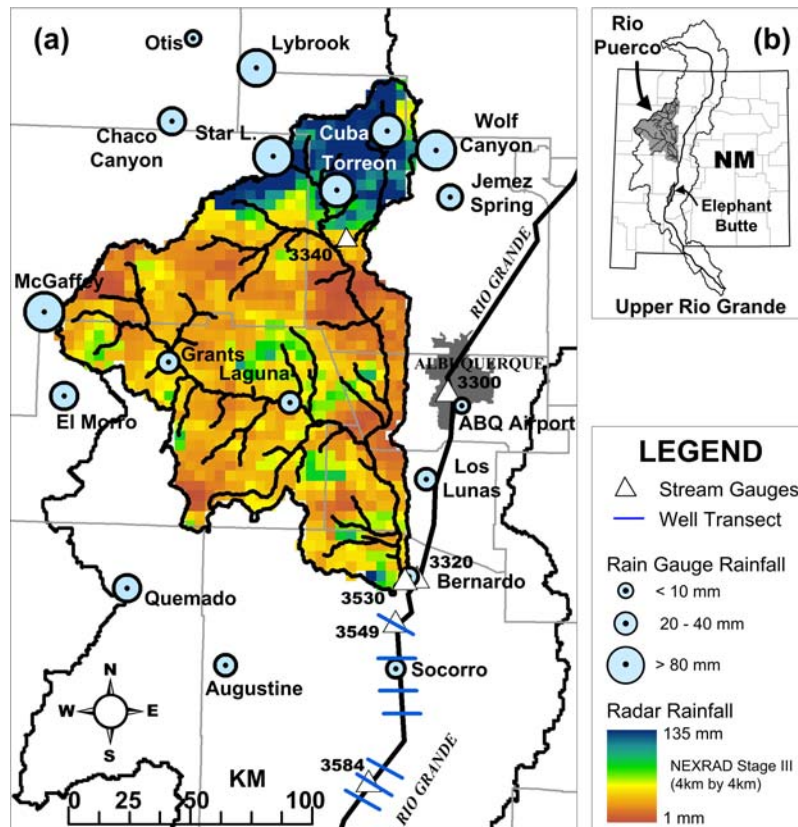


Figure 14. Precipitation estimates for the Río Puerco Watershed Sep 6 – 19 2004

From the USGS discharge data, hydrographs were constructed for gauges both in the basin and along the Río Grande (*Figure 15*). Within the Río Puerco Basin, the flood peak enlarges from Guadalupe to Bernardo suggesting an influx of water from sources other than the Upper Río Puerco. Based upon the rainfall data, this influx probably emanated from the Arroyo Chico subbasin. The Río Grande hydrographs demonstrate minimal flow volumes north of the Río Puerco confluence with larger flood crests at the southern Río Grande gauging stations. Thus the majority of the water contributing to the Río Grande flood can be traced back to the Río Puerco event.

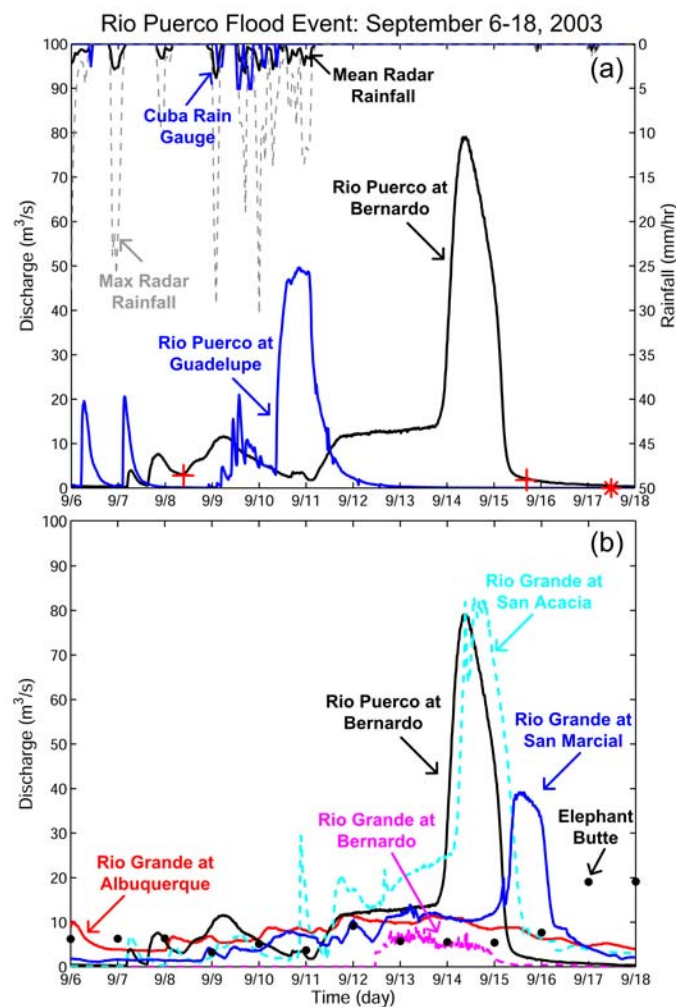


Figure 15. a) Río Puerco at Guadalupe and Río Puerco at Bernardo Hydrographs; Mean Radar Rainfall based upon NEXRAD Stage II hourly data along with maximum single-pixel rainfall depth in the basin. B) Río Grande Hydrographs

This research is an ongoing collaboration between research groups at New Mexico Tech. An article will appear this year in Geophysical Research Letters incorporating the surface components discussed above along with ground water response at well transects along the Río Grande. Future work consists of calibrating the tRIBS model and attempting to simulate this flood event utilizing NEXRAD Stage III data as atmospheric forcing (Please refer to *Part 2* of this report for detailed discussion of calibration efforts).

Part 5. Conclusion

The steps discussed previously will aid in a comprehensive understanding of the effects of climate, land use properties, and soil characteristics on the hydrologic basin response for the Rio Puerco Watershed. Should a more robust relationship between ENSO, PDO, and streamflow in the northern reaches of the basin emerge through more sophisticated statistical techniques, we should be able to predict the variance in future streamflow with increased certainty. In addition, a calibrated tRIBS model for the catchment will allow researchers at New Mexico Tech to alter soil and land use distributions and subsequently observe variations in modeled stream response. Should these results prove comparable with actual trends in streamflow, we will be able to offer a physical explanation for the observed increased precipitation within the basin accompanied by a decrease in annual streamflow.

Part 6. Acknowledgements

I would like to thank the Water Resources Research Institute at New Mexico State University for providing funding that helped to establish the foundations for this research project. I would also like to thank my advisor, Enrique Vivoni, for his patience and advice in my graduate school endeavors. Finally, Robert Gold at the Albuquerque USGS office has been most helpful in providing us with high-resolution streamflow data.

References

- Amarasekera, K.N., R.F. Lee, E.R. Williams, E.A.B. Eltahir, 1997: ENSO and the natural variability in the flow of tropical rivers. *Journal of Hydrology*, **200**, 24–39.
- Dingman, S. Lawrence *Physical Hydrology*. Prentice Hall: Upper Saddle River, NJ. 2002.
- Douglas, M. W., Maddox, R. A., Howard, K., and S. Reyes, The Mexican Monsoon, *J. Climate*, **8**, 1665-1677, 1993.
- Gutzler, D.S., D.M. Kann, and C Thornburgh, 2002: Modulation of ENSO-Based Long-Lead Outlooks of Southwestern U.S. Winter Precipitation by the Pacific Decadal Oscillation. *Weather and Forecasting*, **12**, 1163–1172.
- Ivanov, V.Y., Vivoni, E.R., Bras, R.L., Entekhabi, D., 2004. Catchment hydrologic response with a fully-distributed triangular irregular network mode. *Water Resour. Res.* Submitted for publication.
- Kahya, E. and J.A. Dracup, 1994: The Influences of Type 1 El Niño and La Niña Events on Streamflows in the Pacific Southwest of the United States. *Journal of Climate*, **6**, 965-976.
- Lough J.M. and H.C. Frits: Thou Southern Oscillation and Tree Rings, 1985: 1600 – 1961. *Journal of Climate and Applied Meteorology* (24) 952 – 966.
- Mantua, Nate 2000: *The Pacific Decadal Oscillation*. To appear in The Encyclopedia of Global Environmental Change available at website <http://www.jisao.washington.edu/pdo>
- Minobe, Shoshire 1997: A 50–70 Year Climatic Oscillation over the North Pacific and North America. *Geophysical Research Letters*, **24**(6), 683–686.
- Molnár, Peter and Jorge A. Ramírez, 2001: Recent Trends in Precipitation and Streamflow in the Rio Puerco Basin. *Journal of Climate*, (**5**), 2317-2328.
- Redmond, K.T. and R.W. Koch 1991: Surface Climate and Streamflow Variability in the Western United States and Their Relationship to Large-Scale Circulation Indices. *Water Resources Research*, **27**(9), 2381–2399.
- Swetnam T.W. and J.L Betancourt, 1990: Fire-Southern Oscillation Relations in the Southwestern United States. *Science* (249) 1017 – 1020.
- Vivoni, E.R., Ivanov, V.Y., Bras, R.L., Entekhabi, D., 2004a. Generation of triangulated irregular networks based on hydrological similarity. *J. Hydrol. Eng.* 9(4), 288-303.

Vivoni, E.R., Rhinehart, A.J., Wyckoff, R.L., and Martinez, A., 2004b. Fine-Resolution Hydrologic Modeling: Preliminary Results in the Upper Rio Grande. EOS Poster Abstract No. H33D-0496, AGU Fall Meeting 2004.

Vivoni, E.R., Bowman R.S., Wyckoff R.L., Jakubowski, R.T., Kate R.E., 2004. Analysis of a Monsoon Flood Event in an Ephemeral Tributary to the Río Grande and Its Downstream Effects. To be submitted to Geophysical Research Letters.

Wang, Guiling and Elfatih A. B. Eltahir, 1999: Use of ENSO Information in Medium and Long-Range Forecasting of the Nile Floods. *Journal of Climate*, **12**, 1726–1737.